Optical properties of core/shell spherical quantum dots*

Shuo Li(李硕), Lei Shi(石磊)†, and Zu-Wei Yan(闫祖威)

College of Science, Inner Mongolia Agricultural University, Hohhot 010018, *China*

(Received 4 April 2020; revised manuscript received 20 May 2020; accepted manuscript online 25 May 2020)

In this study, the effects of quantum dot size on the binding energy, radiative lifetime, and optical absorption coefficient of exciton state in both GaN/$Al_xGa_{1-x}N$ core/shell and $Al_xGa_{1-x}N$/GaN inverted core/shell quantum dot structures are studied. For the GaN/$Al_xGa_{1-x}N$ core/shell structure, the variation trend of binding energy is the same as that of radiation lifetime, both of which increase first and then decrease with the increase of core size. For $Al_xGa_{1-x}N$/GaN inverted core/shell structure, the binding energy decreases first and then increases with core size increasing, and the trends of radiation lifetime varying with core size under different shell sizes are different. For both structures, when the photon energy is approximately equal to the binding energy, the peak value of the absorption coefficient appears, and there will be different peak shifts under different conditions.

Keywords: spherical quantum dot, binding energy, optical absorption coefficient, exciton radiation lifetime

PACS: 78.67.Hc, 73.21.La, 71.35.–y **DOI:** 10.1088/1674-1056/ab961a

1. Introduction

Since the 1980s, Rossetti *et al.*[1] have studied the size effect and other relevant properties of CdS nanocrystals, which has attracted people's attention to quantum dots. After that, Peng *et al.*[2] found a simple way to synthesize quantum dots (QDs) on a large scale, enabling many researchers to further study quantum dots. In many quantum dot researches, the third-generation nitride semiconductor quantum dot materials, such as GaN and AlN, have a very broad application prospect in optoelectronic and optical detection devices (blue, green, and ultraviolet light), and high frequency and power laser devices due to their special properties such as wide band gap, high mobility, *etc*.[3–6] Generally speaking, nitride semiconductor materials are divided into wurtzite and zinc blende. The wurtzite and zinc blende have hexagonal and cubic structures respectively, and their properties are different due to different structures. Therefore, many people are interested in comparing the two different properties caused by different structures.[7–10] However, due to the higher crystal symmetry, smaller band gap and higher electron mobility of zinc blende, zinc blende structure is studied by many people.[11–14]

Generally speaking, because excitons can show the electrical and optical properties of quantum dots to a certain extent, many people have done research on excitons in both experiment and theory.[15–17] Chafai *et al.*[18] used the variational method to predict that in the spherical GaN/AlN core/shell quantum dot, the external electric field will reduce the binding energy of exciton state, and the increase of quantum dot size will also reduce the binding energy. Pattammal *et al.*[19] studied the influence of well width on exciton radiation lifetime in InGaN/GaN quantum wires. The results show that the radiation lifetime decreases monotonically with the increase of well width, and the trend becomes more obvious when the well width is smaller. Traetta *et al.*[20] studied the effect of multibody effect on exciton properties in GaN/AlGaN quantum well. The results showed that the built-in electric field caused by spontaneous and piezoelectric polarizations can reduce the exciton state binding energy and optical absorption coefficient. Xia *et al.*[21] considered the influence of the combination of laser field and external electric field on the exciton binding energy of GaN/AlGaN quantum well. It is found that when the applied electric field is small, the laser field will reduce the binding energy and the oscillator strength, however, when the applied electric field is very strong, the binding energy and the oscillator strength first increase and then decrease with the increase of the laser field, and a maximum value appears. Although one has done a lot of researches if the exciton states in some low-dimensional structures, the exciton in the core/shell QD especially in the inverted core/shell QD are lacking, and the comparison of the optical properties between both structures is rarely reported.

In this study, the exciton binding energy, optical absorption coefficient and exciton radiation lifetime for each of both core/shell and inverted core/shell quantum dots are studied by using the variational method under the effective mass approximation. The influence of core and shell sizes on them are studied. The rest of this paper is organized as follows. In Section 2 we present the theoretical framework. In Section 3, we discuss the results of the numerical calculations. Finally, We summarize the main conclusions in Section 4.

*Project supported by the Natural Science Foundation of Inner Mongolia Autonomous Region, China (Grant Nos. 2019MS01006 and 2020MS01008), the Science Project of the Higher Education of Inner Mongolia Autonomous Region, China (Grant No. NJZY19047), the Doctoral Starting-up Foundation of Inner Mongolia Agricultural University, China (Grant No. BJ2013B-2), and the Grassland Talent Project, China.

†Corresponding author. E-mail: shi_lei_family@163.com

2. Theoretical model

In this paper, the spherical GaN/$Al_xGa_{1-x}N$ core/shell and $Al_xGa_{1-x}N$/GaN inverted core/shell QDs are studied. The core radius of the QDs is R_1, and the shell radius is R_2. The Schrödinger equation for an exciton in such a structure is

$$\hat{H}_x = \frac{-\hbar^2}{2m_e^*}\Delta_e + \frac{-\hbar^2}{2m_h^*}\Delta_h + U_e + U_h - \frac{e^2}{4\pi\varepsilon_0\varepsilon^*|\boldsymbol{r}_e - \boldsymbol{r}_h|}, \quad (1)$$

where m_e (m_h) is the effective mass of electron (hole), $\boldsymbol{r}_e$ ($\boldsymbol{r}_h$) is the position vector of electron (hole), e is the absolute value of electronic charge, ε_0 is the dielectric constant of vacuum, and ε^* is the dielectric constant in quantum dot material, and U_e (U_h) is the confining potential of electron (hole).

In this paper, we use the Hylleraas polar system, so the Hamiltonian in Eq. (1) can be written as follows:[22]

$$\begin{aligned}\hat{H}_x = {} & \frac{-\hbar^2}{2m_e^*}\left(\frac{\partial^2}{\partial r_e^2} + \frac{2}{r_e}\frac{\partial}{\partial r_e} + \frac{r_e - r_h + r_{eh}}{r_e r_{eh}} \times \frac{\partial^2}{\partial r_e \partial r_{eh}} + \frac{\partial^2}{\partial r_{eh}^2} + \frac{2}{r_{eh}}\frac{\partial}{\partial r_{eh}}\right) \\ & + \frac{-\hbar^2}{2m_h^*}\left(\frac{\partial^2}{\partial r_h^2} + \frac{2}{r_h}\frac{\partial}{\partial r_h} + \frac{r_h - r_e + r_{eh}}{r_h r_{eh}} \times \frac{\partial^2}{\partial r_h \partial r_{eh}} + \frac{\partial^2}{\partial r_{eh}^2} + \frac{2}{r_{eh}}\frac{\partial}{\partial r_{eh}}\right) \\ & + U_e + U_h - \frac{e^2}{4\pi\varepsilon_0\varepsilon^* r_{eh}}. \end{aligned} \quad (2)$$

The detailed derivation is given in Appendix A. For core/shell structures of QDs (see Fig. 1), the corresponding confining potential is

$$U_{e,h} = \begin{cases} 0, & r_{e,h} \le R_1, \\ V_{e,h}, & R_1 \le r_{e,h} \le R_2, \\ \infty, & r_{e,h} \ge R_2, \end{cases} \quad (3)$$

for inverted core/shell structures of QDs (see Fig. 1), the corresponding confining potential is

$$U_{e,h} = \begin{cases} V_{e,h}, & r_{e,h} \le R_1, \\ 0, & R_1 \le r_{e,h} \le R_2, \\ \infty, & r_{e,h} \ge R_2. \end{cases} \quad (4)$$

In Eqs. (3) and (4), V_e and V_h are the conduction and valence band offsets, respectively (see Fig. 1). The range with $r_{e,h} \ge R_2$ (the outermost layer of the QD) is regarded as a vacuum environment, because the vacuum energy level is much higher than the energy of electron and hole, resulting in very weak tunneling, so the outermost layer is regarded as an infinite high barrier.[23]

Here, we choose the ratio of the conduction band to the valence band to be 6:4, so the barrier height is

$$V_e = 0.6(E_{g(Al_xGa_{1-x}N)} - E_{g(GaN)}), \quad (5)$$

$$V_h = 0.4(E_{g(Al_xGa_{1-x}N)} - E_{g(GaN)}), \quad (6)$$

where the band gap of ternary mixed crystal compound $Al_xGa_{1-x}N$ is

$$E_{g(Al_xGa_{1-x}N)} = (1-x)E_{g(GaN)} + xE_{g(AlN)}. \quad (7)$$

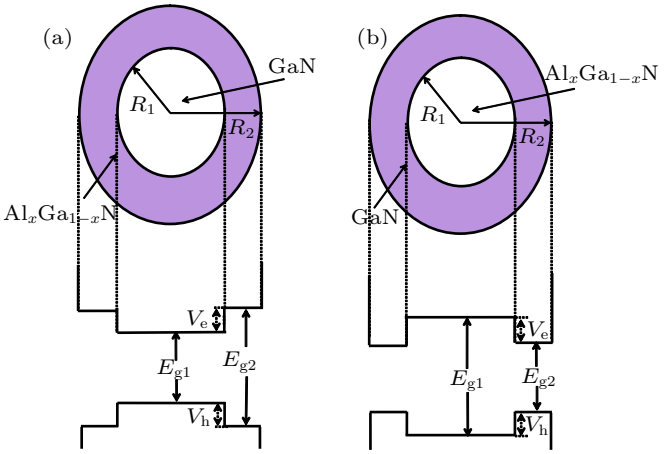

Fig. 1. Core/shell (a) and inverted core/shell (b) structures of QDs.

The effective mass of electron and hole in unit of free electron mass m_0 can be given by

$$m_i^* = \begin{cases} m_{i1}, & r_i < R_1, \\ m_{i2}, & R_1 \le r_i \le R_2, \end{cases} \quad (8)$$

with $i = e,h$, where regardless of the effective mass of electron and hole in either model, the effective mass expressions of electron and hole of ternary mixed crystal compound $Al_xGa_{1-x}N$ are

$$m_e^*(Al_xGa_{1-x}N) = (1-x)m_e^*(GaN) + xm_e^*(AlN), \quad (9)$$

$$m_h^*(Al_xGa_{1-x}N) = (1-x)m_h^*(GaN) + xm_h^*(AlN), \quad (10)$$

where ε^* is the dielectric constant in the quantum dot material, which can take the following form

$$\varepsilon^* = \begin{cases} \varepsilon_1, & r_e \le R_1 \text{ and } r_h \le R_1, \\ \varepsilon_2, & R_1 \le r_e \le R_2 \text{ and } R_1 \le r_h \le R_2, \\ \dfrac{\varepsilon_1 + \varepsilon_2}{2}, & \text{others}. \end{cases} \quad (11)$$

For core/shell structures of QDs (see Fig. 1), the wave functions of electron and hole are[24]

$$\phi_i(r) = \begin{cases} \dfrac{A_{i1}\sin[k_{i1}r_i]}{r_i}, & r_i \le R_1, \\ \dfrac{A_{i2}\sinh[k_{i2}(r_i - R_2)]}{r_i}, & R_1 \le r_i \le R_2, \end{cases} \quad (12)$$

with $i = e,h$, where $k_{i1} = \sqrt{2m_{i1}E_i/\hbar^2}$, and $k_{i2} = \sqrt{2m_{i2}(V_i - E_i)/\hbar^2}$.

For the inverted core/shell structure of QDs (see Fig. 1), the wave functions of electron and hole are[25]

$$\phi_i(r) = \begin{cases} \dfrac{A_{i1}\sinh[k_{i1}r_i]}{r_i}, & r_i \le R_1, \\ \dfrac{A_{i2}\sin[k_{i2}(r_i - R_2)]}{r_i}, & R_1 \le r_i \le R_2, \end{cases} \quad (13)$$

with $i = \mathrm{e,h}$, where $k_{i1} = \sqrt{2m_{i1}(V_i - E_i)/\hbar^2}$, and $k_{i2} = \sqrt{2m_{i2}E_i/\hbar^2}$. In Eqs. (12) and (13), A_{ij} is the normalization coefficient, and E_i is the energy of the ground state, and they can be obtained from the normalization condition and boundary continuity condition.

The exciton ground state wave function Ψ_x and the corresponding ground state energy E_x can be expressed by Schrödinger equation as follows:

$$\hat{H}_x\Psi(r_\mathrm{e}, r_\mathrm{h}, r_\mathrm{eh}) = E_x\Psi(r_\mathrm{e}, r_\mathrm{h}, r_\mathrm{eh}). \tag{14}$$

Because there is no analytical solution for Eq. (14), we determine the wave function by approximate method. Here the trial wave function we choose is

$$\Psi_x(r_\mathrm{e}, r_\mathrm{h}, r_\mathrm{eh}) = \phi_\mathrm{e}(r_\mathrm{e})\phi_\mathrm{h}(r_\mathrm{h})\,\mathrm{e}^{-\lambda r_\mathrm{eh}}, \tag{15}$$

where λ is a variational parameter, the ground state energy of exciton can be obtained by minimizing the expectation energy as follows:

$$E_x = \min_{\lambda} \frac{\langle\Psi_x|H_x|\Psi_x\rangle}{\langle\Psi_x|\Psi_x\rangle}. \tag{16}$$

The binding energy E_b of exciton state is

$$E_\mathrm{b} = E_\mathrm{e} + E_\mathrm{h} - E_x. \tag{17}$$

The optical absorption coefficient (OAC) is defined as:[26]

$$\sigma = \frac{\pi e^2 E_\mathrm{p}}{6nc\varepsilon_0 m_0 \omega V} I_\mathrm{op}\delta(E_\mathrm{b} - \hbar\omega), \tag{18}$$

where c is the velocity of light, n is the refractive index and its value is $\sqrt{\varepsilon^*}$, m_0 represents the free electron mass, I_op is the optical integral part of the radiative transition corresponding to the recombination of electron and hole, and it can be expressed as[27]

$$I_\mathrm{op} = \left|\int \Psi_x(r_\mathrm{e}, r_\mathrm{h}, r_\mathrm{eh})\delta(r_\mathrm{e}, r_\mathrm{h})\,\mathrm{d}V\right|^2. \tag{19}$$

As is usually done, the δ function in Eq. (18) is replaced by a narrow Lorentzian by means of[28]

$$\delta(E_\mathrm{b} - \hbar\omega) = \frac{\Gamma}{\pi\left[(E_\mathrm{b} - \hbar\omega)^2 + \Gamma^2\right]}, \tag{20}$$

where Γ is the line-width of the exciton and its value is 6 meV,[26] E_p is the Kane energy, which is 25 eV for GaN.[29]

The oscillator strength of exciton ground state is expressed as[30]

$$f = \frac{E_\mathrm{p}}{2E_\mathrm{ph}} I_\mathrm{op}. \tag{21}$$

The radiative lifetime is defined as[31,32]

$$\tau = \frac{6\pi\varepsilon_0 m_0 c^3\hbar^2}{e^2 n\beta_\mathrm{s} E_\mathrm{ph}^2 f}, \tag{22}$$

where f is the oscillator strength and E_ph is the interband transition energy, which can be expressed as

$$E_\mathrm{ph} = E_\mathrm{g} + E_x, \tag{23}$$

where E_g is the band gap energy of GaN in this work. β_s is the screening factor, which is shown in Ref. [32] and it can be expressed as

$$\beta_\mathrm{s} = \frac{3\varepsilon}{\varepsilon_\mathrm{NQD} + 2\varepsilon}, \tag{24}$$

where ε and ε_NQD are the optical dielectric constants of shell material and core material, respectively.

3. Results and discussion

In the present paper, GaN/$Al_xGa_{1-x}N$ core/shell and $Al_xGa_{1-x}N$/GaN inverted core/shell QDs are studied. The parameters used are shown in Table 1.

Table 1. Parameters used in calculation.

	$E_\mathrm{g}(0)$/meV	m_e^*	m_h^*	ε^*
GaN	3299[a]	0.15[a]	0.27[b]	10.74[b]
AlN	4900[a]	0.25[a]	0.47[b]	8.41[b]

[a]Ref. [33], [b]Ref. [34].

Figure 2 shows the variation of the binding energy of GaN/$Al_xGa_{1-x}N$ core/shell QD with QD size. It can be seen from the figure that the binding energy of exciton state first increases and then decreases with the increase of core size R_1. This is because when the core size is too small, the quantum tunneling effect for electron and hole is large. And then the average distance between electron and hole becomes large, so the binding energy is small. But with the increase of the core size, the tunneling effect is reduced, and then the average distance between electron and hole decreases, which causes the binding energy to increase, and therefore a maximum value appears. However, as the core size continues to increase, the quantum confinement effect decreases and thus the binding energy decreases. The results are in agreement with those in Refs. [35–37]. In addition, we find that since the electrons and holes are mainly confined to the core region for the core/shell structure, the change of shell size has little effect on the binding energy.

Figure 3 shows the variation of the radiative lifetime and overlap integral I_OP of GaN/$Al_xGa_{1-x}N$ core/shell QD with QD size. Like the scenario in Fig. 2, it can be seen that the radiative lifetime first increases and then decreases with the increase of the core size R_1, and the variation of shell size R_2 has little effect on it. We can know from Eqs. (21) and (22) that the radiative lifetime is inversely proportional to $I_\mathrm{OP} \times E_\mathrm{ph}$. It can be known from the calculation that although the I_OP first

decreases and then increases with the increase of core size as shown in Fig. 3(b), $E_{\rm ph}$ decreases monotonically. Because the sensitivity of radiation lifetime to $I_{\rm OP}$ is higher than to $E_{\rm ph}$, the radiative lifetime first increases and then decreases with the increase of core size, and decreases slightly with the increase of shell size.

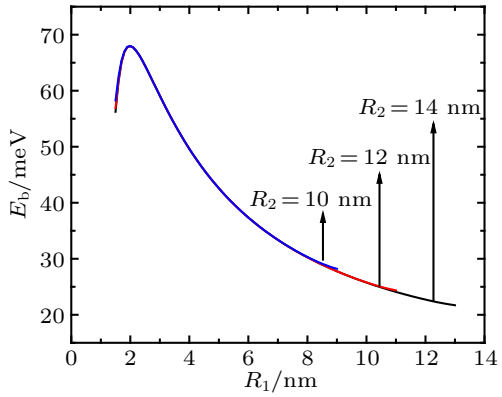

Fig. 2. Plots of binding energy of exciton state in GaN/Al_xGa_{1-x}N core/shell QD *versus* core radius R_1 for different values of shell R_2. The Al content x is chosen to be 0.3.

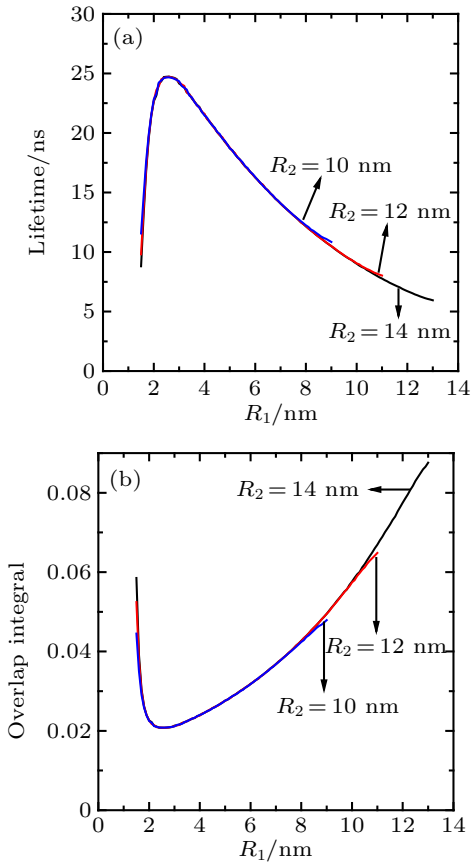

Fig. 3. Variation of (a) radiative lifetime and (b) overlap integral of exciton state in GaN/Al_xGa_{1-x}N core/shell QD with core size R_1 and shell size R_2, with Al content x chosen to be 0.3.

Figure 4(a) shows the variations of the OAC of GaN/Al_xGa_{1-x}N core/shell QD with photon energy under different core sizes. Equation (20) shows that the peak position of PCS appears at $\hbar\omega \approx E_{\rm b}$, and its intensity is related to $I_{\rm OP}/E_{\rm b}$. It can be seen from the figure that the peak intensity of the OAC first decreases and then increases with the increase of core size, and meanwhile the peak position shows a blue-to-red shift. This can be explained as follows. As seen from Figs. 2 and 4(b), although $I_{\rm OP}$ first decreases and then increases with the increase of core size, the binding energy $E_{\rm b}$ first increases and then decreases, which results in the peak shifting from blue to red. As mentioned above, because the intensity of OAC is related to $I_{\rm OP}/E_{\rm b}$, it first decreases and then increases.

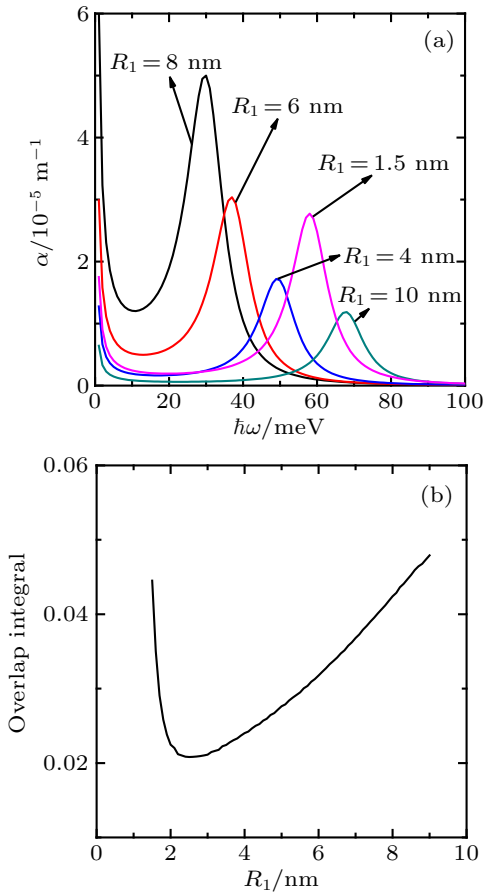

Fig. 4. (a) Variations of OAC of exciton state in GaN/Al_xGa_{1-x}N core/shell QD with photon energy under different values of core size R_1 at shell size $R_2 = 10$ nm, and (b) variation of overlap integral of exciton state in GaN/Al_xGa_{1-x}N core/shell QD with core size R_1 at $R_2 = 10$ nm, with Al content x chosen to be 0.3.

Figure 5 shows the variations of the binding energy of Al_xGa_{1-x}N/GaN inverted core/shell QD with QD size. It can be seen from the figure that the binding energy of exciton state first decreases and then increases with the increase of core size R_1. This is because for the inverted core/shell structure, electron and hole are mainly confined in the shell region. As the core size increases, the distance between electron and hole increases under the repulsion of the barrier V_0, which leads the binding energy to decrease. However, as the core size continues to increase, the quantum tunneling effect becomes important, which leads the electron and hole to tunnel into the core region, resulting in the decrease of the distance

between electron and hole, therefore the binding energy increases. In addition, it is clearly shown that the change of shell size R_2 in the $Al_xGa_{1-x}N$/GaN inverted core/shell structure has more obvious effect on the binding energy than that in the GaN/$Al_xGa_{1-x}N$ core/shell structure (see Fig. 2), and for a fixed core size, the binding energy decreases with the increase of the shell size due to the quantum confinement effect decreasing. The results are in agreement with those in Ref. [38].

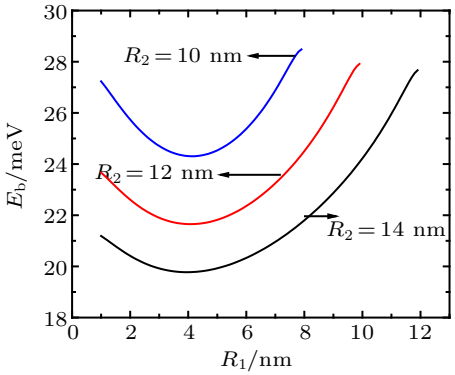

Fig. 5. Variations of binding energy of exciton state in $Al_xGa_{1-x}N$/GaN inverted core/shell QD with core size R_1 for different values of shell size R_2, with Al content x chosen to be 0.3.

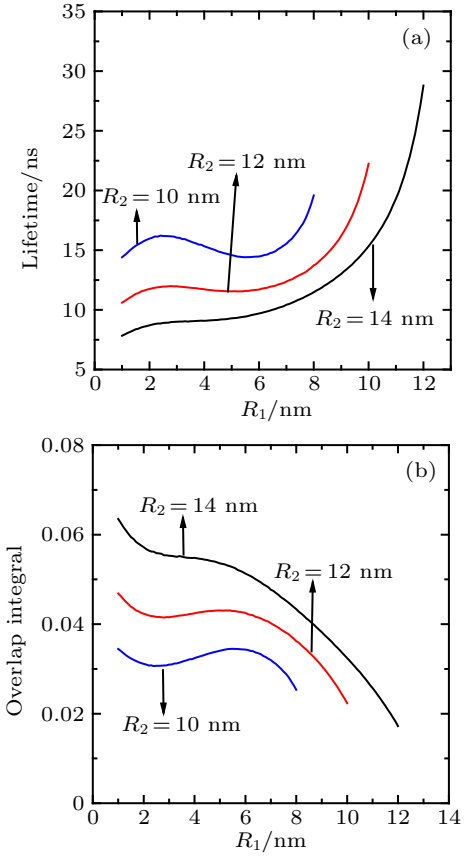

Fig. 6. Variations of (a) radiative lifetime and (b) overlap integral of exciton state in $Al_xGa_{1-x}N$/GaN inverted core/shell QD with core size R_1 for different values of shell size R_2, with Al content x chosen to be 0.3.

Figure 6(a) shows the variations of the radiative lifetime of $Al_xGa_{1-x}N$/GaN inverted core/shell QD with QD size. It can be seen from the figure that the variation trend of radiation lifetime with the core size is obviously different under different shell sizes. When $R_2 = 10$ nm and 12 nm, the radiation lifetimes each show a nonmonotonic variation trend. However, when $R_2 = 14$ nm, the radiation lifetime increases monotonically with the increase of the core size. As for I_{OP}, its variation trend is opposite to that of the radiation lifetime as explained before.

Figure 7(a) shows the variations of the OAC with photon energy under different core sizes. It can be seen from the figure that the peak intensity of the OAC first decreases, then increases, and again decreases with the increase of core size. This behavior is the same as that of I_{op}. As explained before, because the OAC is more sensitive to I_{op} than E_b, leading to this result. Moreover, the E_b first decreases and then increases, which results in the peak position of OAC shifting from red to blue as shown in the figure.

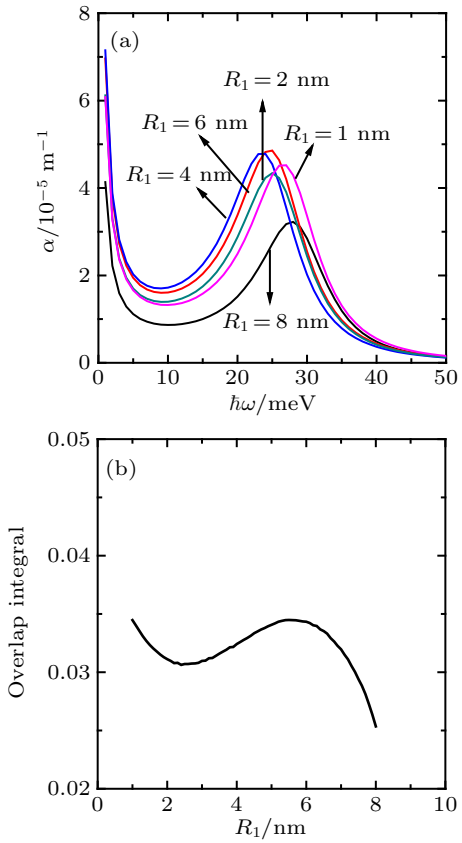

Fig. 7. (a) Variations of OAC of exciton state in $Al_xGa_{1-x}N$/GaN inverted core/shell QD with photon energy for different values of core size R_1 at $R_2 = 10$ nm (a), and (b) variastion of overlap integral of exciton state in $Al_xGa_{1-x}N$/GaN inverted core/shell QD with the core size R_1 at $R_2 = 10$ nm (b), with Al content x chosen to be 0.3.

4. Conclusions

In the present work, the effects of QD size on the binding energy, the radiative lifetime, and the OAC of exciton state in both GaN/$Al_xGa_{1-x}N$ core/shell and $Al_xGa_{1-x}N$/GaN inverted core/shell QD structures are studied. For the GaN/$Al_xGa_{1-x}N$ core/shell structure, the binding energy and radiative lifetime first increase and then decrease with the in-

crease of core size, but only when the core size is very big, will the variation of shell size have a distinguishable effect on the binding energy and the radiative lifetime of exciton state in this structure. In contrast, for the $Al_xGa_{1-x}N$/GaN inverted core/shell structure, the binding energy first decreases and then increases with the increase of core size, but the variation trends of radiation lifetime are obviously different under different shell sizes, and both of the binding energy and the radiative lifetime decrease with the increase of shell size. Moreover, in both of the different structures, the peak position of the OAC occurs at $\hbar\omega \approx E_b$, and not only red shift but also blue shift occurs The peak intensity of the OAC first decreases and then increases with the increase of core size for GaN/$Al_xGa_{1-x}N$ core/shell QD structure, however, it first decreases , then increases, and again decreases with the increase of core size for $Al_xGa_{1-x}N$/GaN inverted core/shell QD structure. We hope that the present work will provide some useful references for the research of QD optoelectronic devices, such as how to choose the size and structure of devices to improve the OAC and radiative lifetime of exciton.

Appendix A: The derivation of Hamiltonian (2)

The following expressions are the derivation of Hamiltonian (2) in the Hylleraas coordinate system.

$$r_1^2 = x_1^2 + y_1^2 + z_1^2, \tag{A1}$$

$$r_2^2 = x_2^2 + y_2^2 + z_2^2, \tag{A2}$$

$$r_{12}^2 = (x_1 - x_2)^2 + (y_1 - y_2)^2 + (z_1 - z_2)^2. \tag{A3}$$

$$\frac{\partial \Psi}{\partial x_1} = \frac{\partial \Psi}{\partial r_1}\frac{x_1}{r_1} + \frac{\partial \Psi}{\partial r_{12}}\frac{x_1 - x_2}{r_{12}}, \tag{A4}$$

$$\begin{aligned}\frac{\partial^2 \Psi}{\partial x_1^2} = {} & \frac{\partial^2 \Psi}{\partial r_1^2}\frac{x_1^2}{r_1^2} + \frac{\partial \Psi}{\partial r_1}\left(\frac{1}{r_1} - \frac{x_1^2}{r_1^3}\right) + \frac{\partial^2 \Psi}{\partial r_{12}^2}\frac{(x_1 - x_2)^2}{r_{12}^2} \\ & + \frac{\partial \Psi}{\partial r_{12}}\left(\frac{1}{r_{12}} - \frac{(x_1 - x_2)^2}{r_{12}^3}\right) \\ & + 2\frac{\partial^2 \Psi}{\partial r_1 \partial r_{12}}\frac{x_1(x_1 - x_2)}{r_1 r_{12}}.\end{aligned} \tag{A5}$$

According to Eq. (A5), a similar equation can be obtained as follows:

$$\frac{\partial^2 \Psi}{\partial y_1^2} = \frac{\partial^2 \Psi}{\partial r_1^2}\frac{y_1^2}{r_1^2} + \frac{\partial \Psi}{\partial r_1}\left(\frac{1}{r_1} - \frac{y_1^2}{r_1^3}\right) + \frac{\partial^2 \Psi}{\partial r_{12}^2}\frac{(y_1 - y_2)^2}{r_{12}^2} + \frac{\partial \Psi}{\partial r_{12}}\left(\frac{1}{r_{12}} - \frac{(y_1 - y_2)^2}{r_{12}^3}\right) + 2\frac{\partial^2 \Psi}{\partial r_1 \partial r_{12}}\frac{y_1(y_1 - y_2)}{r_1 r_{12}}, \tag{A6}$$

$$\frac{\partial^2 \Psi}{\partial z_1^2} = \frac{\partial^2 \Psi}{\partial r_1^2}\frac{z_1^2}{r_1^2} + \frac{\partial \Psi}{\partial r_1}\left(\frac{1}{r_1} - \frac{z_1^2}{r_1^3}\right) + \frac{\partial^2 \Psi}{\partial r_{12}^2}\frac{(z_1 - z_2)^2}{r_{12}^2} + \frac{\partial \Psi}{\partial r_{12}}\left(\frac{1}{r_{12}} - \frac{(z_1 - z_2)^2}{r_{12}^3}\right) + 2\frac{\partial^2 \Psi}{\partial r_1 \partial r_{12}}\frac{z_1(z_1 - z_2)}{r_1 r_{12}}. \tag{A7}$$

Therefore,

$$\begin{aligned}\frac{\partial^2 \Psi}{\partial x_1^2} + \frac{\partial^2 \Psi}{\partial y_1^2} + \frac{\partial^2 \Psi}{\partial z_1^2} = {} & \frac{\partial^2 \Psi}{\partial r_1^2}\frac{r_1^2}{r_1^2} + \frac{\partial \Psi}{\partial r_1}\left(\frac{3}{r_1} - \frac{r_1^2}{r_1^3}\right) + \frac{\partial^2 \Psi}{\partial r_{12}^2}\frac{r_{12}^2}{r_{12}^2} + \frac{\partial \Psi}{\partial r_{12}}\left(\frac{3}{r_{12}} - \frac{r_{12}^2}{r_{12}^3}\right) \\ & + 2\frac{\partial^2 \Psi}{\partial r_1 \partial r_{12}}\frac{x_1(x_1 - x_2) + y_1(y_1 - y_2) + z_1(z_1 - z_2)}{r_1 r_{12}},\end{aligned} \tag{A8}$$

where

$$\begin{aligned}2\frac{\partial^2 \Psi}{\partial r_1 \partial r_{12}}\frac{x_1(x_1 - x_2) + y_1(y_1 - y_2) + z_1(z_1 - z_2)}{r_1 r_{12}} &= \frac{\partial^2 \Psi}{\partial r_1 \partial r_{12}}\frac{2x_1^2 + 2y_1^2 + 2z_1^2 - 2x_1x_2 - 2y_1y_2 - 2z_1z_2}{r_1 r_{12}} \\ &= \frac{\partial^2 \Psi}{\partial r_1 \partial r_{12}}\frac{2x_1^2 + 2y_1^2 + 2z_1^2 - 2x_1x_2 - 2y_1y_2 - 2z_1z_2 + (x_2^2 + y_2^2 + z_2^2) - (x_1^2 + y_1^2 + z_1^2)}{r_1 r_{12}} \\ &= \frac{\partial^2 \Psi}{\partial r_1 \partial r_{12}}\frac{x_1^2 + y_1^2 + z_1^2 + (x_1 - x_2)^2 + (y_1 - y_2)^2 + (z_1 - z_2)^2 - (x_1^2 + y_1^2 + z_1^2)}{r_1 r_{12}} \\ &= \frac{\partial^2 \Psi}{\partial r_1 \partial r_{12}}\frac{r_1^2 - r_2^2 + r_{12}^2}{r_1 r_{12}}.\end{aligned} \tag{A9}$$

Therefore,

$$\frac{\partial^2 \Psi}{\partial x_1^2} + \frac{\partial^2 \Psi}{\partial y_1^2} + \frac{\partial^2 \Psi}{\partial z_1^2} = \frac{\partial^2 \Psi}{\partial r_1^2}\frac{r_1^2}{r_1^2} + \frac{\partial \Psi}{\partial r_1}\left(\frac{3}{r_1} - \frac{r_1^2}{r_1^3}\right) + \frac{\partial^2 \Psi}{\partial r_{12}^2}\frac{r_{12}^2}{r_{12}^2} + \frac{\partial \Psi}{\partial r_{12}}\left(\frac{3}{r_{12}} - \frac{r_{12}^2}{r_{12}^3}\right) + 2\frac{\partial^2 \Psi}{\partial r_1 \partial r_{12}}\frac{r_1^2 - r_2^2 + r_{12}^2}{r_1 r_{12}}. \tag{A10}$$

It can also be written as

$$\Delta_1 = \frac{\partial^2 \Psi}{\partial r_1^2} + \frac{2}{r_1}\frac{\partial \Psi}{\partial r_1} + \frac{r_1^2 - r_2^2 + r_{12}^2}{r_1 r_{12}}\frac{\partial^2 \Psi}{\partial r_1 \partial r_{12}} + \frac{\partial^2 \Psi}{\partial r_{12}^2} + \frac{2}{r_{12}}\frac{\partial \Psi}{\partial r_{12}}. \tag{A11}$$

References

[1] Rossetti R, Nakahaha S and Brus L E 1983 *J. Chem. Phys.* **79** 1086
[2] Peng Z A and Peng X 2001 *J. Am. Chem. Soc.* **123** 183
[3] Akita K, Kyono T, Yoshizumi Y, Kitabayashi H and Katayama K 2007 *J. Appl. Phys.* **101** 033104
[4] Khan M A, Shatalov M, Maruska H P, Wang H M and Kuokstis E 2005 *Jpn. J. Appl. Phys.* **44** 7191
[5] Ruf T, Serrano J, Cardona M, Pavone P, Pabst M, Krisch M, D'Astuto M, Suski T, Grzegory I and Leszczynski M 2011 *Phys. Rev. Lett.* **86** 906
[6] Zeiri N, Bouazra A, Abdi-Ben Nasrallah S and Said M 2020 *Phys. Scr.* **95** 045801
[7] Fonoberov V A and Balandin A A 2003 *J. Appl. Phys.* **94** 7178
[8] Balandin A A and Fonoberov V A 2004 *J. Vac. Sci. Technol. B* **22** 2190
[9] Cheng T S, Jenkins L C, Hooper S E, Foxon C T, Orton J W and Lacklison D E 1995 *Appl. Phys. Lett.* **66** 1509
[10] Raya-Moreno M, Rurali R and Cartoixà X 2019 *Phys. Rev. Mater.* **3** 084607
[11] Ghazi El H and Pete A J 2017 *Superlattices and Microstructures* **104** 222
[12] Ben Afkir N, Feddi E, Dujardin F, Zazoui M and Meziane J 2018 *Physica B: Condensed Matter* **534** 10
[13] Tang Z M, Liu J H, Liu Y L, He H, Fu Y C and Shen X M 2019 *IOP Conf. Series: Materials Science and Engineering* **504** 012080
[14] Wang H Y, Jin G and Tan Q L 2019 *IOP Conf. Series: Materials Science and Engineering* **563** 022009
[15] Shan L, Agarwal M and Mishchenko E G 2019 *Phys. Rev. B* **99** 035434
[16] Andreev A D and O'Reilly E P 2001 *Appl. Phys. Lett.* **79** 521
[17] Muth J F, Lee J H, Shmagin I K, Kolbas R M, Casey H C, Casey Jr H C, Keller B P, Mishraand U K and DenBaars S P 1997 *Appl. Phys. Lett.* **71** 2572
[18] Chafai A, Essaoudi I, Ainane A, Dujardin F and Ahuja R 2019 *Physica B* **559** 23
[19] Pattammal M, John Peter A and Yoo Chang Kyoo 2011 *Superlattices and Microstructures* **50** 181
[20] Traetta G, Cingolani R, Carlo A Di, Sala F D and Lugli P 2000 *Appl. Phys. Lett.* **76** 1042
[21] Xia C X, Chen X Y, Wei S Y and Jia Y 2013 *J. Appl. Phys.* **113** 214310
[22] Hylleraas E A 1929 *Z. Physik* **54** 347
[23] Adachi S 2005 *Properties of Group IV, III–V and II–VI Semiconductors* (England: Wiley) pp. 195–198
[24] Shi L and Yan Z W 2019 *J. Appl. Phys.* **125** 174302
[25] Ibral A, Zouitine A, Aazou S, Assaid El Mahdi, Feddi El Mustapha and Dujardin F 2013 *J. Optoelectron. Adv. Mater.* **15** 1268
[26] El-Yadri M, Feddi E, Aghoutane N, El Aouami A, Radu A, Dujardin F, Nguyen Chuong V, Phuc Huynyh V and Duque C A 2018 *J. Appl. Phys.* **124** 144303
[27] Alen B, Bosch J, Granados D, Martínez-Pastor J, García J M and González L 2007 *Phys. Rev. B* **75** 045319
[28] Anchala, Purohit S P and Mathur K C 2012 *IEEE J. Quantum Electron.* **48** 628
[29] Marquardt O, Mourad D, Schulz S, Hickel T, Czycholl G and Neugebauer J 2008 *Phys. Rev. B* **78** 235302
[30] Bosch J, Alén B, Martinez-Pastor J, Granados D, Garcia J M and González L 2008 *Superlattices and Microstructures* **43** 582
[31] Califano M, Franceschetti A and Zunger A 2007 *Phys. Rev. B* **75** 115401
[32] Aktürk A, Sahin M, Koc F and Erdinc A 2014 *J. Phys. D: Appl. Phys.* **47** 285301
[33] Vurgaftman I, Meyer J R and Ram-Mohan L R 2001 *J. Appl. Phys.* **89** 5815
[34] Lei L P, Shi L and Yan Z W 2019 *Journal of Inner Mongolia University* (Natural Science Edition) **50** 2
[35] Senger R T and Bajaj K K 2003 *Phys. Rev. B* **68** 205314
[36] Mathan Kumar K, John Peter A and Lee C 2011 *Eur. Phys. J. B* **84** 431
[37] Narayanan M and John Peter A 2012 *Superlattices and Microstructures* **51** 486
[38] Khamkhami J El, Feddi E, Assaid E, Dujardin F, Stebe B and Diouri J 2002 *Physica E* **15** 99